Journal of Molecular Modeling (2018) 24: 150
https://doi.org/10.1007/s00894-018-3686-8

ORIGINAL PAPER

Binding of indomethacin methyl ester to cyclooxygenase-2. A computational study

Menyhárt-Botond Sárosi [1]

Received: 23 December 2017 / Accepted: 21 May 2018 / Published online: 5 June 2018

Abstract

Inhibitors selective towards the second isoform of prostaglandin synthase (cyclooxygenase, COX-2) are promising nonsteroidal anti-inflammatory drugs and antitumor medications. Methylation of the carboxylate group in the relatively nonselective COX inhibitor indomethacin confers significant COX-2 selectivity. Several other modifications converting indomethacin into a COX-2 selective inhibitor have been reported. Earlier experimental and computational studies on neutral indomethacin derivatives suggest that the methyl ester derivative likely binds to COX-2 with a similar binding mode as that observed for the parent indomethacin. However, docking studies followed by molecular dynamics simulations revealed two possible binding modes in COX-2 for indomethacin methyl ester, which differs from the experimental binding mode found for indomethacin. Both alternative binding modes might explain the observed COX-2 selectivity of indomethacin methyl ester.

Keywords Indomethacin derivatives · Cyclooxygenase · Protein-ligand binding · Docking simulations · Molecular dynamics

Introduction

Prostaglandin synthase (cyclooxygenase, COX) plays a key role in the biosynthesis of prostanoids. COX has two isoforms with similar structure and high sequence identity [1]. The COX-1 isoform is expressed constitutively whereas COX-2 is induced mainly by pathological processes and would be an ideal target for nonsteroidal anti-inflammatory drugs (NSAIDs). In contrast to nonselective NSAIDs, COX-2 selective inhibitors exhibit fewer side effects and are promising antitumor drug candidates [2]. The design of COX-2 selective inhibitors exploits the differences in size and flexibility of the binding sites of the two COX isoforms [2, 3]. Due to a V523 to I523 substitution, substitutions in the secondary shell (R513 to H513 and V434 to I434) and the relative shift of the membrane binding domain (MBD) resulting in displacement of R120, the solvent accessible surface in the COX-2 active site is larger than that in COX-1 [4]. Furthermore, substitutions in the amino acid sequences of the two COX isoforms result in higher flexibility of the COX-2 binding site [2, 3]. The homodimeric COX enzymes behave as heterodimers during inhibition, and communication between the COX monomers has been observed [5]. The NSAID indomethacin is relatively nonselective [6, 7]. However, conversion of the carboxylate group into the neutral methyl ester confers COX-2 selectivity (**1**; Fig. 1) [3, 6].

The binding mode of indomethacin in COX-2 is known from protein crystallography [Protein Data Bank (PDB) ID: 4COX Fig. 2a] [8], but no crystal structure of COX-2 complexed with **1** has been published to date. However, site-directed mutagenesis studies have revealed different trends for the binding of carboxylate NSAIDs compared to the neutral compounds [3]. The binding of the carboxylic acid-containing indomethacin requires interactions with both R120 and Y355. On the other hand, COX-2 inhibition by neutral NSAID derivatives (i.e., indomethacin amides and esters) is unaffected by mutations of R120 [3]. These indomethacin derivatives are expected to interact primarily with constriction site residues Y355 and Q524 [3, 9]. Furthermore, COX selectivity and binding of indomethacin ethanolamide derivatives is enantiomer

This paper belongs to Topical Collection 11th European Conference on Theoretical and Computational Chemistry (EuCO-TCC 2017)

Electronic supplementary material The online version of this article (https://doi.org/10.1007/s00894-018-3686-8) contains supplementary material, which is available to authorized users.

✉ Menyhárt-Botond Sárosi
menyhart.sarosi@uni-leipzig.de

[1] Faculty of Chemistry and Mineralogy, Institute of Inorganic Chemistry, Leipzig University, Johannisallee 29, 04103 Leipzig, Germany

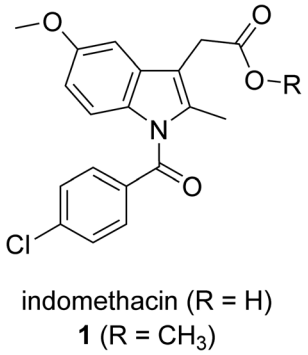

indomethacin (R = H)
1 (R = CH_3)

Fig. 1 Indomethacin and its methyl ester (**1**)

dependent (see Supporting Information, Fig. S1) [10–12]. The lack of a time-dependent inhibition behavior towards COX-1 and a low affinity towards COX-1 due to the lack of a free carboxylate group might explain the COX-2 selectivity of indomethacin *R*-ethyl-ethanolamide [12–14]. A COX-2 crystal structure complexed with a carborane derivative of **1** was published recently (Fig. 2b). The replacement of the 4-chlorophenyl ring in **1** with the anionic 7,8-*nido*-dicarbaborate preserves the high COX-2-selective inhibitory activity and improves solubility and stability of the drug molecule [15]. The PDB ID: 4Z0L crystal structure revealed a binding mode different from that of indomethacin but somewhat similar to the binding mode of indomethacin *S*-ethyl-ethanolamide in COX-1. The COX-2 structure itself showed certain notable features in the 4Z0L structure. The *nido* cluster resides in a hydrophobic pocket opened up by the rotation of the L531 side chain and the MBD showed significant structural flexibility [15]. L531 exhibits similar rotation upon binding of NSAIDs of the oxicam family [16, 17].

The various modifications made to indomethacin clearly affected the resulting binding mode. Earlier experimental and computational studies for neutral indomethacin derivatives suggest that compound **1** likely binds to COX-2 with a binding mode similar to that observed for indomethacin [11, 12]. However, alternative binding modes for **1** cannot be excluded and need to be verified. Molecular dynamics (MD) simulations have been shown to be useful for verifying the viability of alternative binding modes observed during docking calculations and might be useful to determine the most stable binding mode for the COX-2 selective inhibitor **1**. A previously unreported alternative binding mode in COX-2 for the bromo-phenyl analogue of celecoxib was found during metadynamics simulations. The alternative binding mode explained well the experimental observations particular to this type of inhibitor [18].

Computational methods

Docking studies

Ligand structures were constructed with GaussView 5 [19]. Ligand geometries were optimized with Gaussian 09 at the HF/6-31G(d,p) level of theory [20]. The atomic charges for each ligand were derived using the RESP procedure [21–23] with Gaussian 09 and the *antechamber* program of the AmberTools13 package [24]. The crystal structures of COX-2 complexed with the COX-2-selective inhibitors celecoxib (PDB ID: 3LN1) [25] and the 7,8-*nido*-dicarbaborate derivative of indomethacin methyl ester (PDB ID: 4Z0L) [15] were downloaded from the PDB. All ligands and non-standard residues except for the heme groups, and all water molecules were removed with the UCSF Chimera package [26]. Protonation of the cysteine residues forming disulfide bonds was corrected where necessary. One homodimer of both COX-2 structures was prepared for docking with AutoDock Tools 1.5.6 [27]. After adding the missing hydrogen atoms to the selected protein structures, all polar hydrogen atoms were kept and all non-polar hydrogen atoms were merged in order to conform to the AutoDock atom types. Simultaneously, Gasteiger charges were also assigned to each atom of the two macromolecules, since the AutoDock4 scoring function

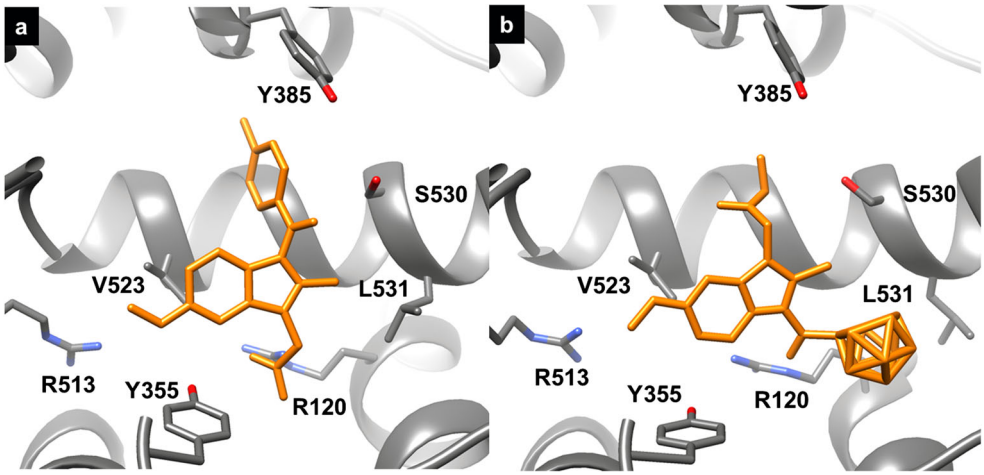

Fig. 2 **a** Crystal structure of indomethacin in COX-2 (PDB 4COX). **b** Crystal structure of the *nido*-carborane derivative of **1** in COX-2 (PDB 4Z0L). *R* Arginine, *Y* tyrosine, *S* serine, *L* leucine, *V* valine

was calibrated using Gasteiger partial charges on both the ligand and the macromolecule [27]. All histidine, lysine and arginine residues were set up in their protonated state, whereas all aspartic acid and glutamic acid residues were set up in their deprotonated state. The optimized geometries of the ligands were prepared for docking. Ligand nonpolar hydrogens were merged to conform to the AutoDock atom types. The docking area was defined using AutoGrid 4.2.5 [27]. A 60 × 44 × 44 Å three-dimensional (3D) affinity grid with 0.375 Å grid point spacing was placed around the COX-2 active site including relevant parts of the corresponding MBD. Docking was performed with AutoDock 4.2.5.1 [27]. A ligand conformational search was performed using the Lamarckian genetic algorithm (LGA) [28]. One hundred docking runs starting from random initial positions and conformations were carried out with the following LGA parameters: 150 individuals, 4×10^6 energy evaluations, 27,000 generations, elitism of 1, 0.02 mutation rate, 0.8 crossover rate, local search frequency of 0.06 and 300 iterations per local search. The clustering of the final docked conformations was carried out with a tolerance of a root-mean-square deviation (RMSD) of 1.5 Å. The setup of the docking protocols and the analysis of the results were performed with AutoDock Tools 1.5.6 [27]. The standard error of the AutoDock free energy scoring function was 2–3 kcal mol^{-1} [27].

Molecular mechanics and MD simulations

The crystallographic water molecules found in the 3LN1 PDB file were retained. The ff99SB force field [29] was assigned to the COX residues. The ligand coordinates were taken from the docking simulations, and ligand hydrogen atoms were added automatically with the UCSF Chimera package [26]. The general AMBER force field for organic molecules (GAFF) was used to describe the ligands [30]. The heme force field parameters were taken from the work of Furse et al. [31]. A weak harmonic restraint of 20 kcal mol^{-1} $Å^{-2}$) was defined between the heme iron atom and the HIS-388 NE2 atom in both COX-2 monomers [10]. Each protein-ligand structure was immersed in a pre-equilibrated SPC/E truncated octahedral water box [32]. The SPC/E solvent boxes extended at least 11 Å from the solute and included the crystallographic water molecules. The *sander* program of the Amber12 package [24] was used for molecular mechanics (MM) minimizations and MD simulations. Three minimization steps were carried out before the MD simulations. First: 100 steps of steepest descent and 200 steps of conjugate gradient minimization of the solute molecules (solvent atoms were held fixed). Second: 300 steps of steepest descent and 700 steps of conjugate gradient minimization of the solvent molecules (solute atoms were held fixed). Third: 100 steps of steepest descent and 200 steps of conjugate gradient minimization of both solvent and solute molecules without any restraints. Next, with a 2 kcal mol^{-1} $Å^{-2}$ restraint on the solute atoms, a two-step MD simulation was carried out. First: over a period of 50 ps, each system was heated from 0 to 300 K in the canonical (NVT) ensemble. Second: over a period of 50 ps, each system was relaxed at $T = 300$ K and $P = 1$ atm in the isothermic-isobaric (NPT) ensemble. Subsequently, 5 ns MD simulations were run in the NPT ensemble ($T = 300$ K and $P = 1$ atm) without any restraints and saving the atomic coordinates every 5 ps. A 9 Å cutoff for nonbonded interactions was used during force calculations with periodic boundary conditions. SHAKE was used to constrain the bonds with hydrogen atoms [33]. In order to maintain the system temperature, a Langevin thermostat with a collision frequency of 3 ps^{-1} was employed [34]. All MD simulations employed a timestep of 2 fs. Production MD simulations for additional 100 ns were carried out with the GPU accelerated *pmemd* implementation of the *sander* program [35–37]. Atom coordinates were saved every 200 ps. Every restart of the MD simulations altered the random number generator seed [38]. Further analysis of the trajectories was carried out using *cpptraj* [39].

MM/Poisson–Boltzmann surface area calculations

MM/Poisson–Boltzmann surface area (MM/PBSA) binding free energies were calculated with the *MMPBSA.py* program [40] averaging over every collected snapshot of the last 80 ns. In the first set, the MM/PBSA calculations used the same atomic radii as the MM and MD simulations. In the second set, the atom-type/charge-based radii optimized for the AMBER atom types were used for the receptor [41]. The iron ions and porphyrin residues and the corresponding parameters were discarded for the second set of MM/PBSA calculations. The ligand radii were the same as the radii used for the MM and MD simulations. The total non-polar solvation free energy was modeled as two terms throughout: the cavity term and the dispersion term [42, 43]. Normal mode calculations were not carried out, since the systems in question are of similar entropy.

Results and discussion

Docking of **1** into COX-2:celecoxib crystal structure (PDB 3LN1) revealed three possible binding modes (Fig. 3). The lowest energy docked pose (Fig. 3, Pose 1) was similar to the binding mode of indomethacin from PDB 4COX. The second lowest energy docked pose (Fig. 3, Pose 2) was similar to the binding mode of the 7,8-*nido*-dicarbaborate-derivative from PDB 4Z0L, the 4-chlorophenyl moiety of **1** pointing towards L531. The indole moiety of the third docked orientation (Fig. 3, Pose 3) is flipped along the amide bond compared to both Pose 1 and the experimental binding mode of the relatively nonselective indomethacin. The ester group in

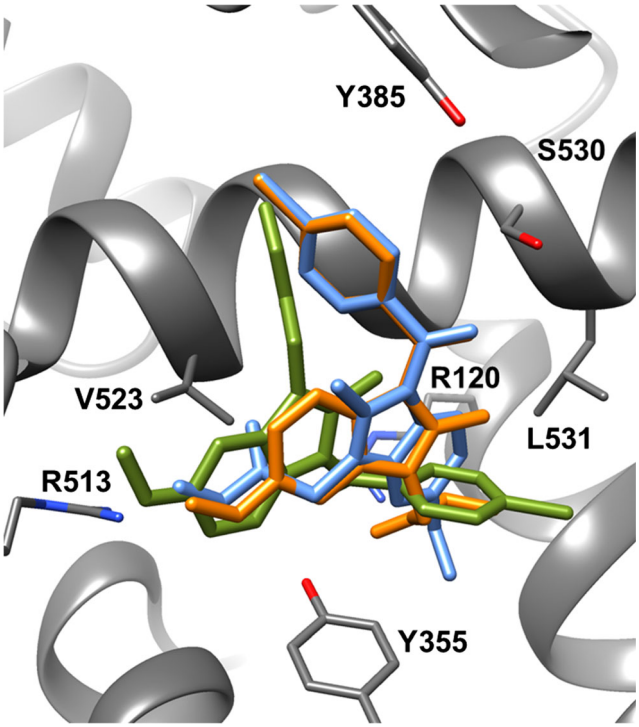

Fig. 3 **1** docked into COX-2 (PDB 3LN1). *Orange* Pose 1, *green* Pose 2, *blue* Pose 3

Pose 3 forms polar interactions with R513 instead of R120. Similar predictions have been obtained from docking simulations using the PDB 4Z0L crystal structure (Fig. S2a). Naturally, the differences between the two COX-2 structures somewhat influenced the outcome of the docking predictions. However, the predicted overall interaction patterns between COX-2 and **1** were very similar from both docking simulations. The 4-chlorophenyl group of **1** in Pose 2 readily occupies the hydrophobic sub-pocket in the PDB 4Z0L structure, and the carboxylate ester group of **1** in Pose 3 reaches more easily the R513 residue, compared to the docking poses obtained with the PDB 3LN1 structure.

In Pose 2, the methoxy group protrudes into the side pocket near V523 and might explain the COX-2 selectivity of **1** compared to indomethacin. The bulkier I523 residue in COX-1 might make the binding of **1** in this orientation less favorable compared to COX-2. In Pose 1, the methoxy group does not protrude so deep into the side pocket near V523. Furthermore, the relatively nonselective inhibitor indomethacin binds to COX-2 in an orientation similar to Pose 1. Pose 3 might also explain the high COX-2 selectivity of **1** compared to the parent indomethacin, since residue 513 is a histidine in COX-1. COX-1 H513 does not reach as far into the COX active site as COX-2 R513 does and might not be able to form a hydrogen bond with the methyl ester group of **1**. Furthermore, the bulkier I523 residue in COX-1 could restrict access to the side pocket [4].

Docking of indomethacin carboxylate into the 3LN1 COX-2 structure did not predict any interaction between the carboxylic acid moiety and R513. Only the experimental binding mode found in PDB 4COX and the alternative orientation similar to the binding mode of the 7,8-*nido*-dicarbaborate-derivative from PDB 4Z0L have been identified for the indomethacin carboxylate (see Fig. S2b).

MD simulations have been carried out using the COX-2:celecoxib structure (PDB ID: 3LN1) in order to verify the predictions obtained from the docking simulations. The ligand atoms fluctuated considerably more during the 105 ns MD simulation started from Pose 1, compared to the other two trajectories (Fig. 4). Pose 2 and Pose 3 showed smaller ligand atom fluctuations and an overall higher stability during the whole 105 ns MD simulations compared to Pose 1. The values are only slightly lower for Pose 3 compared to Pose 2. All three orientations showed relatively similar ligand atom fluctuations during the last 80 ns, Pose 1 being again an exception. The fluctuation of the COX-2 backbone atoms showed a relative stability for all three systems (see Fig. S3). However, the different orientation of the ligand resulted in different trends. The MD simulations started from both Pose 1 and Pose 2 resulted in rather similar backbone atom fluctuations of both COX-2 monomers. The backbone atoms of the COX-2 monomer complexed with **1** in Pose 3 showed higher fluctuations during the 105 ns MD simulations compared to the other two systems. On the other hand, the backbone atoms of the

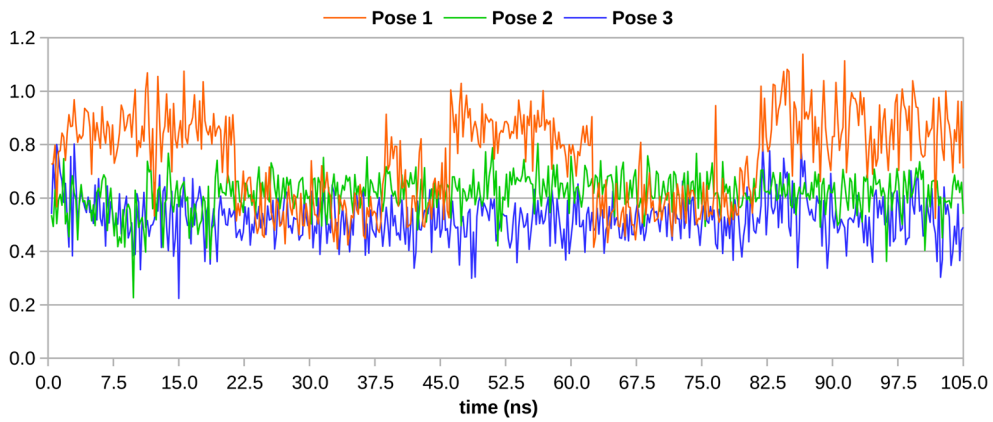

Fig. 4 Root-mean-square deviation of all internal distance pairs (dRMSD, in Å) of **1** from 105 ns molecular dynamics (MD) simulations started from the three different orientations

Table 1 Binding free energies (ΔG_{bind}) in kcal mol^{-1} for the last 80 ns simulations obtained from the two sets of MM/PBSA calculations. Standard deviations are in parentheses

	ΔE_{MM} [a]	ΔG_{sol} [b]	ΔG_{bind} [c]
1st set			
Pose 1	−59.94 (7.25)	61.48 (9.10)	1.54 (4.72)
Pose 2	−70.64 (5.61)	73.82 (4.91)	3.18 (5.29)
Pose 3	−79.08 (3.56)	81.90 (3.44)	2.82 (3.86)
2nd set			
Pose 1	−60.20 (7.02)	54.99 (6.83)	−5.21 (4.30)
Pose 2	−70.60 (5.67)	64.43 (3.77)	−6.16 (5.10)
Pose 3	−78.66 (3.54)	68.54 (3.33)	−10.12 (4.12)

[a] Gas phase molecular mechanical energy change

[b] Desolvation free energy change.

[c] $\Delta E_{MM} + \Delta G_{sol}$

"empty" partner monomer showed similar fluctuations during the MD simulations started from all three orientations of **1**, especially during the last 80 ns.

The last 80 ns MD trajectories were used for the MM/PBSA binding free energy calculations (Table 1). Based on the gas phase molecular mechanical energy change (ΔE_{MM}), Pose 3 is clearly favored over the other two orientations. However, the desolvation free energy (ΔG_{sol}) gave completely different trends depending on the setup of the calculations (see Computational Methods). The first set of MM/PBSA

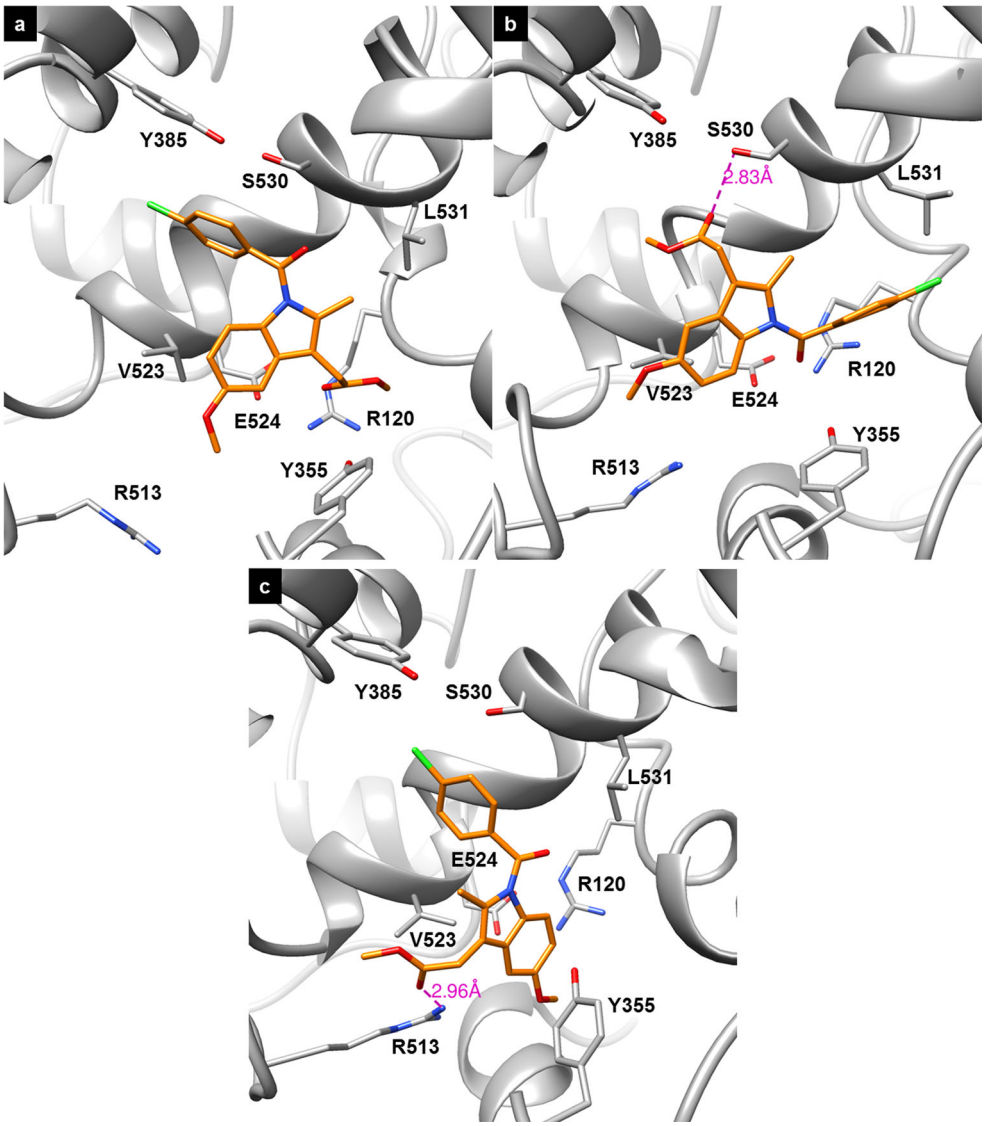

Fig. 5 Coordinates taken from the last frame of the 105 ns MD simulations started from **a** Pose 1, **b** Pose 2 and **c** Pose 3. COX-2 C atoms and ribbon: *gray,* **1** C atoms: *orange*, *N atoms: blue*, *O atoms: red*, *Cl atoms: green*. Hydrogen atoms are not shown for clarity. Selected hydrogen bonds are shown in Å

calculations did not favor the binding of **1** to COX-2 in any of the three poses. On the other hand, the second set of MM/PBSA calculations clearly favored Pose 3 over the other two orientations. The standard deviation was similar for all three systems (Table 1). It has been shown that the performance of standard MM/PBSA methods is strongly dependent on the atomic radii and varies with the tested system; the effects from binding-site water molecules are neglected [44, 45].

The MD simulations started from Pose 1 revealed no long-lived hydrogen bonds between **1** and COX-2 residues (Fig. 5a). The methyl-ester group of **1** formed only intermittent hydrogen bonds with R120. Furthermore, the fluctuation of the methyl-ester group of **1** most probably resulted in the large ligand RMSD values (Fig. 4). The carbonyl group of **1** formed a hydrogen bond with S530 only during the first ~10 ns. The 4-chlorophenyl moiety and the methoxy group of **1** interacted with COX-2 Y385 and V523, respectively, and with surrounding residues.

During the 105 ns MD run started from Pose 2, the carbonyl group of **1** formed intermittent hydrogen bonds with Y355 whereas the carboxyl methyl-ester of **1** formed a long-lived hydrogen bond with S530 (Fig. 5b). The 4-chlorophenyl moiety of **1** in Pose 2 points towards L531 and forces it to rotate away during the 105 ns MD run. The same displacement of L531 has been observed in the crystal structure of COX-2 complexed with the 7,8-*nido*-dicarbaborate-derivative of **1** [15] and upon binding of NSAIDs of the oxicam family [16, 17]. Similar to the 7,8-*nido*-dicarbaborate in the PDB 4Z0L structure, the 4-chlorophenyl group of **1** forms mainly hydrophobic interactions with the COX-2 residues in the newly opened side pocket (Fig. 5). Due to the higher flexibility of the COX-2 binding site compared to the COX-1, isoform **1** oriented according to Pose 2 might be more easily accommodated into COX-2 and might explain the observed COX-2 selectivity of **1** [2, 3, 15].

The methyl-ester moiety of **1** formed a hydrogen bond with R513 during the 105 ns MD run started from Pose 3 (Fig. 5c). During the last ~70 ns, the indole moiety of **1** formed a OH···π interaction with Y355. The 4-chlorophenyl group interacted with COX-2 Y385 and surrounding residues. Due to the structural differences between COX-1 and COX-2, Pose 3 might also explain the observed COX-2 selectivity of **1**. The bulkier I523 residue in COX-1 could restrict access to the side pocket around residue 513. Furthermore, H513 in COX-1 does not reach as far into the COX active site as COX-2 R513.

Conclusion

Although earlier experimental and computational studies for neutral indomethacin derivatives suggested a binding mode for **1** similar to the experimental binding mode of the parent indomethacin [11, 12], docking of **1** into multiple COX-2 crystal structures revealed two additional plausible binding modes. Subsequent 105 ns long MD simulations predicted for the orientation of **1** similar to the experimental binding mode of indomethacin in COX-2 the largest ligand atom fluctuations and the least favorable electrostatic and van der Waals interactions with COX-2. Instead, the 105 ns long MD simulations identified both alternative poses as viable binding modes in COX-2 for **1**. Pose 2 is similar to the experimental binding mode of the 7,8-*nido*-dicarbaborate-derivative of **1**. The higher flexibility of the COX-2 binding site compared to the COX-1 isoform might explain the observed COX-2 selectivity of **1** [2, 3, 15]. **1** oriented according to Pose 2 might be more easily accommodated into COX-2 than into COX-1. However, Pose 3 might be also a valid binding mode in COX-2 for **1**. The stabilizing polar interaction of **1** oriented according to Pose 2 with COX-2 R513 is not viable in the COX-1 isoform due to the different amino acid sequences of the two isoforms and also might explain the observed COX-2 selectivity of **1**. Furthermore, in both Pose 2 and Pose 3, **1** formed stabilizing interactions with residues other than R120 and its binding to COX-2 would probably not be affected by mutations of R120, in accordance with site-directed mutagenesis studies of neutral NSAIDs [3].

Acknowledgments This work was supported by the European Union, the Free State of Saxony, and the German Research Foundation (DFG, SA 2902/2-1). Some of the computations were performed on a Bull Cluster at the Center for Information Services and High Performance Computing (ZIH) at Technische Universität Dresden. Molecular graphics were rendered using UCSF Chimera [26]. M-B.S. is grateful to Prof. Dr. Evamarie Hey-Hawkins and Prof. Terry P. Lybrand for their collaboration and support.

References

1. Simmons DL, Botting RM, Hla T (2004) Cyclooxygenase isozymes: the biology of prostaglandin synthesis and inhibition. Pharmacol Rev 56:387–437. https://doi.org/10.1124/pr.56.3.3
2. Michaux C, Charlier C (2004) Structural approach for COX-2 inhibition. Mini-Rev Med Chem 4:603–615. https://doi.org/10.2174/1389557043403756
3. Kalgutkar AS, Crews BC, Rowlinson SW et al (2000) Biochemically based design of cyclooxygenase-2 (COX-2) inhibitors: facile conversion of nonsteroidal antiinflammatory drugs to potent and highly selective COX-2 inhibitors. Proc Natl Acad Sci USA 97:925–930. https://doi.org/10.1073/pnas.97.2.925
4. Blobaum AL, Marnett LJ (2007) Structural and functional basis of cyclooxygenase inhibition. J Med Chem 50:1425–1441. https://doi.org/10.1021/jm0613166
5. Sidhu RS, Lee JY, Yuan C, Smith WL (2010) Comparison of cyclooxygenase-1 crystal structures: cross-talk between monomers comprising cyclooxygenase-1 homodimers. Biochemistry 49:7069–7079. https://doi.org/10.1021/bi1003298

6. Kalgutkar AS, Marnett AB, Crews BC et al (2000) Ester and amide derivatives of the nonsteroidal antiinflammatory drug, indomethacin, as selective cyclooxygenase-2 inhibitors. J Med Chem 43: 2860–2870. https://doi.org/10.1021/jm000004e
7. Hess S, Teubert U, Ortwein J, Eger K (2001) Profiling indomethacin impurities using high-performance liquid chromatography and nuclear magnetic resonance. Eur J Pharm Sci 14:301–311. https://doi.org/10.1016/S0928-0987(01)00198-1
8. Kurumbail RG, Stevens AM, Gierse JK et al (1996) Structural basis for selective inhibition of cyclooxygenase-2 by anti-inflammatory agents. Nature 384:644–648. https://doi.org/10.1038/384644a0
9. Konkle ME, Blobaum AL, Moth CW et al (2016) Conservative secondary shell substitution in cyclooxygenase-2 reduces inhibition by indomethacin amides and esters via altered enzyme dynamics. Biochemistry 55:348–359. https://doi.org/10.1021/acs.biochem.5b01222
10. Kozak KR, Prusakiewicz JJ, Rowlinson SW, Marnett LJ (2002) Enantiospecific, selective cyclooxygenase-2 inhibitors. Bioorg Med Chem Lett 12:1315–1318. https://doi.org/10.1016/S0960-894X(02)00133-6
11. Moth CW, Prusakiewicz JJ, Marnett LJ, Lybrand TP (2005) Stereoselective binding of indomethacin ethanolamide derivatives to cyclooxygenase-1. J Med Chem 48:3613–3620. https://doi.org/10.1021/jm0494164
12. Harman CA, Turman MV, Kozak KR et al (2007) Structural basis of enantioselective inhibition of cyclooxygenase-1 by *S*-α-substituted indomethacin ethanolamides. J Biol Chem 282: 28096–28105. https://doi.org/10.1074/jbc.M701335200
13. Gierse JK, Koboldt CM, Walker MC et al (1999) Kinetic basis for selective inhibition of cyclo-oxygenases. Biochem J 339:607–614. https://doi.org/10.1042/bj3390607
14. Walker MC, Kurumbail RG, Kiefer JR et al (2001) A three-step kinetic mechanism for selective inhibition of cyclo-oxygenase-2 by diarylheterocyclic inhibitors. Biochem J 357:709–718. https://doi.org/10.1042/bj3570709
15. Neumann W, Xu S, Sárosi MB et al (2016) *nido*-Dicarbaborate induces potent and selective inhibition of cyclooxygenase-2. Chem Med Chem 11:175–178. https://doi.org/10.1002/cmdc.201500199
16. Xu S, Hermanson DJ, Banerjee S et al (2014) Oxicams bind in a novel mode to the cyclooxygenase active site via a two-water-mediated H-bonding network. J Biol Chem 289:6799–6808. https://doi.org/10.1074/jbc.M113.517987
17. Xu S, Rouzer CA, Marnett LJ (2014) Oxicams, a class of nonsteroidal anti-inflammatory drugs and beyond. IUBMB Life 66:803–811. https://doi.org/10.1002/iub.1334
18. Limongelli V, Bonomi M, Marinelli L et al (2010) Molecular basis of cyclooxygenase enzymes (COXs) selective inhibition. Proc Natl Acad Sci USA 107:5411–5416. https://doi.org/10.1073/pnas.0913377107
19. Dennington R, Keith T, Millam J (2009) GaussView. Semichem Inc., Shawnee Mission, KS
20. Frisch MJ, Trucks GW, Schlegel HB et al (2009) Gaussian 09, Revision A.02. Gaussian, Inc., Wallingford
21. Singh UC, Kollman PA (1984) An approach to computing electrostatic charges for molecules. J Comput Chem 5:129–145. https://doi.org/10.1002/jcc.540050204
22. Besler BH, Merz KM, Kollman PA (1990) Atomic charges derived from semiempirical methods. J Comput Chem 11:431–439. https://doi.org/10.1002/jcc.540110404
23. Bayly CI, Cieplak P, Cornell W, Kollman PA (1993) A well-behaved electrostatic potential based method using charge restraints for deriving atomic charges: the RESP model. J Phys Chem 97: 10269–10280. https://doi.org/10.1021/j100142a004
24. Case DA, Darden TA, Cheatham III TE et al (2012) AMBER 13. University of California, San Francisco
25. Wang JL, Limburg D, Graneto MJ et al (2010) The novel benzopyran class of selective cyclooxygenase-2 inhibitors. Part 2: the second clinical candidate having a shorter and favorable human half-life. Bioorg Med Chem Lett 20:7159–7163. https://doi.org/10.1016/j.bmcl.2010.07.054
26. Pettersen EF, Goddard TD, Huang CC et al (2004) UCSF chimera—a visualization system for exploratory research and analysis. J Comput Chem 25:1605–1612. https://doi.org/10.1002/jcc.20084
27. Morris GM, Huey R, Lindstrom W et al (2009) AutoDock4 and AutoDockTools4: automated docking with selective receptor flexibility. J Comput Chem 30:2785–2791. https://doi.org/10.1002/jcc.21256
28. Morris GM, Goodsell DS, Halliday RS et al (1998) Automated docking using a Lamarckian genetic algorithm and an empirical binding free energy function. J Comput Chem 19:1639–1662. https://doi.org/10.1002/(SICI)1096-987X(19981115)19:14<1639::AID-JCC10>3.0.CO;2-B
29. Hornak V, Abel R, Okur A et al (2006) Comparison of multiple amber force fields and development of improved protein backbone parameters. Proteins 65:712–725. https://doi.org/10.1002/prot.21123
30. Wang J, Wolf RM, Caldwell JW et al (2004) Development and testing of a general amber force field. J Comput Chem 25:1157–1174. https://doi.org/10.1002/jcc.20035
31. Furse KE, Pratt DA, Porter NA, Lybrand TP (2006) Molecular dynamics simulations of arachidonic acid complexes with cox-1 and cox-2: insights into equilibrium behavior. Biochemistry 45: 3189–3205. https://doi.org/10.1021/bi052337p
32. Berendsen HJC, Grigera JR, Straatsma TP (1987) The missing term in effective pair potentials. J Phys Chem 91:6269–6271. https://doi.org/10.1021/j100308a038
33. Ryckaert J-P, Ciccotti G, Berendsen HJ (1977) Numerical integration of the Cartesian equations of motion of a system with constraints: molecular dynamics of n-alkanes. J Comput Phys 23: 327–341. https://doi.org/10.1016/0021-9991(77)90098-5
34. Izaguirre JA, Catarello DP, Wozniak JM, Skeel RD (2001) Langevin stabilization of molecular dynamics. J Chem Phys 114: 2090–2098
35. Götz AW, Williamson MJ, Xu D et al (2012) Routine microsecond molecular dynamics simulations with AMBER on GPUs. 1. Generalized born. J Chem Theory Comput 8:1542–1555. https://doi.org/10.1021/ct200909j
36. Salomon-Ferrer R, Götz AW, Poole D et al (2013) Routine microsecond molecular dynamics simulations with AMBER on GPUs. 2. Explicit solvent particle mesh Ewald. J Chem Theory Comput 9: 3878–3888. https://doi.org/10.1021/ct400314y
37. Le Grand S, Götz AW, Walker RC (2013) SPFP: speed without compromise—a mixed precision model for GPU accelerated molecular dynamics simulations. Comput Phys Commun 184:374–380. https://doi.org/10.1016/j.cpc.2012.09.022
38. Cerutti DS, Duke R, Freddolino PL et al (2008) A vulnerability in popular molecular dynamics packages concerning Langevin and Andersen dynamics. J Chem Theory Comput 4:1669–1680. https://doi.org/10.1021/ct8002173
39. Roe DR, Cheatham TE (2013) PTRAJ and CPPTRAJ: software for processing and analysis of molecular dynamics trajectory data. J Chem Theory Comput 9:3084–3095. https://doi.org/10.1021/ct400341p
40. Miller BR, McGee TD, Swails JM et al (2012) MMPBSA.py: an efficient program for end-state free energy calculations. J Chem Theory Comput 8:3314–3321. https://doi.org/10.1021/ct300418h

41. Tan C, Yang L, Luo R (2006) How well does Poisson–Boltzmann implicit solvent agree with explicit solvent? A quantitative analysis. J Phys Chem B 110:18680–18687. https://doi.org/10.1021/jp063479b
42. Tan C, Tan Y-H, Luo R (2007) Implicit nonpolar solvent models. J Phys Chem B 111:12263–12274. https://doi.org/10.1021/jp073399n
43. Floris F, Tomasi J (1989) Evaluation of the dispersion contribution to the solvation energy. A simple computational model in the continuum approximation. J Comput Chem 10:616–627. https://doi.org/10.1002/jcc.540100504
44. Hou T, Wang J, Li Y, Wang W (2010) Assessing the performance of the MM/PBSA and MM/GBSA methods. 1. The accuracy of binding free energy calculations based on molecular dynamics simulations. J Chem Inf Model 51:69–82. https://doi.org/10.1021/ci100275a
45. Genheden S, Ryde U (2015) The MM/PBSA and MM/GBSA methods to estimate ligand-binding affinities. Expert Opin Drug Discovery 10: 449–461. https://doi.org/10.1517/17460441.2015.1032936